Electrical Power and Energy Systems 155 (2024) 109616

Contents lists available at ScienceDirect

International Journal of Electrical Power and Energy Systems

journal homepage: www.elsevier.com/locate/ijepes

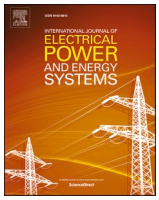

Integrating discrete wavelet transform with neural networks and machine learning for fault detection in microgrids

Antonio Cano [a], Paul Arévalo [a], Darío Benavides [b], Francisco Jurado [a,*]

[a] Department of Electrical Engineering, University of Jaen, 23700 EPS Linaes, Jaén, Spain
[b] Department of Electrical Engineering, University of Málaga, 29010 Málaga, Spain

ARTICLE INFO

Keywords:
Microgrids
Fault detection
Machine learning
Discrete Wavelet transform
Artificial neural network

ABSTRACT

Microgrids are essential for integrating renewable energy sources into the power grid. However, fault detection is challenging due to bidirectional energy flow. Traditional relay-based systems struggle in microgrids, primarily because of limited fault currents from grid-connected renewable energy inverters. To address these challenges, this paper proposes a new methodology for fault detection and classification in a renewable microgrid. The main contributions encompass two key aspects. Firstly, it enhances fault detection performance in microgrids characterized by nonlinear relationships, including photovoltaic, hydrokinetic, and variable electric load systems. Secondly, the combination of the discrete wavelet transform with various types of neural networks and supervised learning techniques provides a robust methodology for fault detection and classification. The proposed approach is evaluated using an IEEE-5 feeder test bed representing a realistic ring network configuration. The results show that the radial basis function neural network model exhibited promising outcomes, yielding a low prediction error of 1.31 e-31, highlighting its practical potential for enhancing system reliability and performance. Furthermore, various test cases were conducted by altering the ground resistance to train the neural networks, demonstrating the effectiveness of this neural network in accurately identifying fault conditions. Additionally, this research achieved promising outcomes with other models, including support vector machine and nonlinear autoregressive with external input, emphasizing the adaptability of these models in fault detection.

1. Introduction

The remarkable growth of renewable energy is being driven by the increasing costs and limited availability of fossil fuels [1]. Smart grids, particularly microgrids (MGs), have played a significant role in accelerating the development of renewable sources. MGs are systems for distributing electricity that consist of distributed generators and loads. These systems can operate both while connected to the main grid and in standalone mode [2]. MGs offer numerous benefits, including cost reduction, high energy quality, and enhancing the reliability of the system for end users [3]. However, they also come with challenges, particularly in managing bidirectional power flow with the main grid. These challenges involve various aspects, such as implementation, operation, control, and MG protection [4]. Conventional systems for detecting faults based on relays are ineffective when applied to MGs. This is because they are designed to detect high levels of fault currents, while the fault currents contributed by grid-connected inverters of renewable sources in MGs are extremely small. Consequently, the protection schemes remain inactive, leaving the MG vulnerable and compromising its reliability and safety. As a result, the development of new methods for detecting and categorizing faults in electrical power systems (EPS) that include MGs has become essential. This paper aims to address this key objective. The bidirectional energy flow between MGs and the grid poses a challenge, as existing protection schemes become redundant. Moreover, MGs with generators of different capacities and types produce fault currents at varying levels, leading to a significant degradation of protection coordination [5]. Traditional overcurrent protection techniques become less suitable as fault currents differ depending on whether the MGs are connected to the main grid or operating in island mode. Therefore, an effective protection system should encompass fault detection, classification, and estimating the location of the fault [6]. This paper primarily concentrates on fault detection and classification, since localizing the fault comes into play once the fault is definitively detected and its type is determined.

* Corresponding author.
E-mail address: fjurado@ujaen.es (F. Jurado).

https://doi.org/10.1016/j.ijepes.2023.109616
Received 23 June 2023; Received in revised form 6 September 2023; Accepted 23 October 2023

In the existing literature, several studies have been conducted on fault detection and classification in MGs. For instance, a method for detecting faults using a differential relay is presented in Ref. [7]. However, this method is expensive and suffers from the aforementioned limitations. In recent years, researchers have predominantly employed techniques based on artificial neural networks (ANNs) and Traveling-Wave (TW) for fault detection in EPS and MGs [8]. These methods offer rapid fault detection, as demonstrated in Ref. [9], where a fault detection method utilizing TW analysis is proposed for DC MGs. Although DC MGs possess advantages over AC MGs, the latter are more common. Nevertheless, applying the TW method to AC MGs presents challenges in detecting the traveling wave head for fault diagnosis [10]. To overcome this limitation, various methods have been proposed for extracting information about the front of the traveling wave. These include Fourier Transform (FT) [11], Fast Fourier Transform (FFT) [12], Singular Value Decomposition (SVD) [11], Hilbert Huang Transform (HHT) [13], and Discrete Wavelet Transform (DWT) [14]. FT and DWT are widely adopted in digital signal processing for analyzing time–frequency signals and extracting their characteristics [14]. The features obtained through these methods are then used un estimation models. Different estimation models have been proposed, such as Support Vector Machine (SVM) [15], Extreme Learning Machine (ELM) [16], Random Forest (RF) [17], Gaussian Process Regression (GPR) [18], and ANN [19]. A comprehensive study on fault detection and classification schemes for MGs can be found in [2], as well as in [5]. A review of this studies is also presented in [6]. Most estimation methods rely on machine learning techniques, with SVM and ANN being the most applied approaches [20].

In contrast to ANN, SVM-based techniques have demostrated greater asuccess in classification and regression analysis applications. However, due to their high computational complexity and the absence of probabilistic estimates, they are less accurate in applications involving parameter estimation with uncertainty. Thus, the most promising methods currently involve combining ANN and DWT. Some studies have proposed such combinations for fault analysis in MGs. For example, Ref. [21] introduces a fault localization model based on Adaptive Neuro-Fuzzy Inference System (ANFIS), using DWT to extract effective and relevant fault current characteristics. The results are encouraging due to the improved optimization algorithm of ANFIS, which prevents convergence to a local optimum. Nevertheless, the computational effort and fault detection speed of the proposed model are not thoroughly addressed in the study. Ref. [9] presents a fault detection model for MGs that utilizes DWT and SVM, covering both radial and ring network configuration, showing promising outcomes. However, the study overlooks the role of renewable sources and focuses solely on DC-based MGs. Additionally, Ref. [14] introduces an intelligent fault detection scheme for AC-based microgrids that incorporates DWT and deep neural networks (DNN). The renewable generators in this case consist of multiple photovoltaic (PV) systems. The results are compared with novel detection and classification methods, demonstrating the superiority of the proposed approach. However, no comparative analysis with other ANN architectures is provided, which could further enhance the system's performance for the same configuration. The Radial Basis Function Neural Network (RBFNN) stands out as a copelling choice for various scientific and technological applications, particularly in the detection of high impedance faults in MGs, due to its flexibility, generalization capability, computational efficiency, adaptability, and interpretability [10]. A study investigates fault detection in an MG comprising PV and wind turbines (WT) using a combination of DWT and RBFNN. The system is simulated using the IEEE 13-node radial test configuration, and the results demonstrate the method's superiority in detecting various fault types, including high impedance faults [10]. The combination of ANN and DWT is crucial because DWT alone struggles to characterize faults in MGs, as the wavelet coefficients change if the fault occurs in a different region of the system. Therefore, employing ANN is essential to enhance fault classification during detection. However, the investigation of fault detection combining DWT and RBFNN in a ring system is overlooked in the study. Furthermore, most studies focus on specific ANN models to validate their approaches and do not extensively explore the wide range of existing ANN architectures. The contribution of fault currents from a renewable system comprising hydrokinetic turbines (HKT), has not been extensively studied. Considering multiple HKT turbines could yield different and unexpected results, making it crucial to investigate their impact. Therefore, despite extensive research into fault detection and classification schemes in MGs, several research gaps persist in this field, as outlined below:

- Although the combination of ANN with DWT has shown promising results for fault detection and classification in MGs, there is a lack of conclusive evidence regarding the superiority of specific ANN architectures. Comparative analyses among multiple ANN architectures for the same MG configuration are essential to determine the most effective approach. For example, in [21], the optimization method of the ANFIS needs improvement to enhance efficiency and avoid local optima. However, it is necessary to explore alternative ANN models that may yield similar or even superior results. The performance and effectiveness of an ANN can vary depending on the specific application and training it receives.
- Fault diagnosis and classification in MGs present challenges due to the difficulty in collecting sufficient data to train the ANN, often resulting in models getting trapped in local minima. To address these limitations and escape local optima, chaotic ANNs offer error handling capabilities and associative memory [22].
- The consideration of MG topology is crucial. While a chaotic ANN is applied in [10] to detect and classify faults in a radial feeder, many MGs are interconnected in a ring configuration as part of the main distribution network. The presence of multiple interconnected lines alters the selectivity of protections and presents new challenges.
- Most articles tend to overlook or disregard the diversity of renewable sources beyond PV and WT within MGs, or they focus solely on one type of source. In future smart grids, the integration of various renewable sources such as HKT, variable loads, and hybrid systems is expected. Therefore, it is essential to evaluate and model the behavior of these diverse sources in ring networks configuration and study their collective response to faults.

This paper introduces a fault detection and classification approach in MGs by combining chaotic neural networks and DWT. The method is applied to a renewable system comprising PV/HKT and variable load. The system is evaluated on an IEEE-5 test bench, which represents a ring network configuration to simulate realistic fault detection scenarios. The system simulation is conducted using Matlab-Simulink. Generally, the contributions are detailed below.

- In response to the research gap concerning the lack of conclusive evidence regarding the superiority of specific ANN architectures in MG fault detection, this paper conducts a comprehensive comparative analysis. Multiple ANN models and machine learning techniques are evaluated within the context of MG fault detection, shedding light on their varying performance in the specific MG configuration considered. This analysis extends beyond the application of a single ANN model, providing valuable insights into the effectiveness of alternative models, thus contributing to filling this gap.
- Addressing the challenge of ANN models getting trapped in local minima due to limited data, this research introduces the use of chaotic ANNs. These chaotic ANNs offer advanced error handling capabilities and associative memory, providing a potential solution to escape local optima during fault diagnosis and classification in microgrids. This novel approach offers an innovative perspective to mitigate this research gap.
- In recognition of the critical importance of MG topology, especially in interconnected ring configurations, this study focuses on a realistic

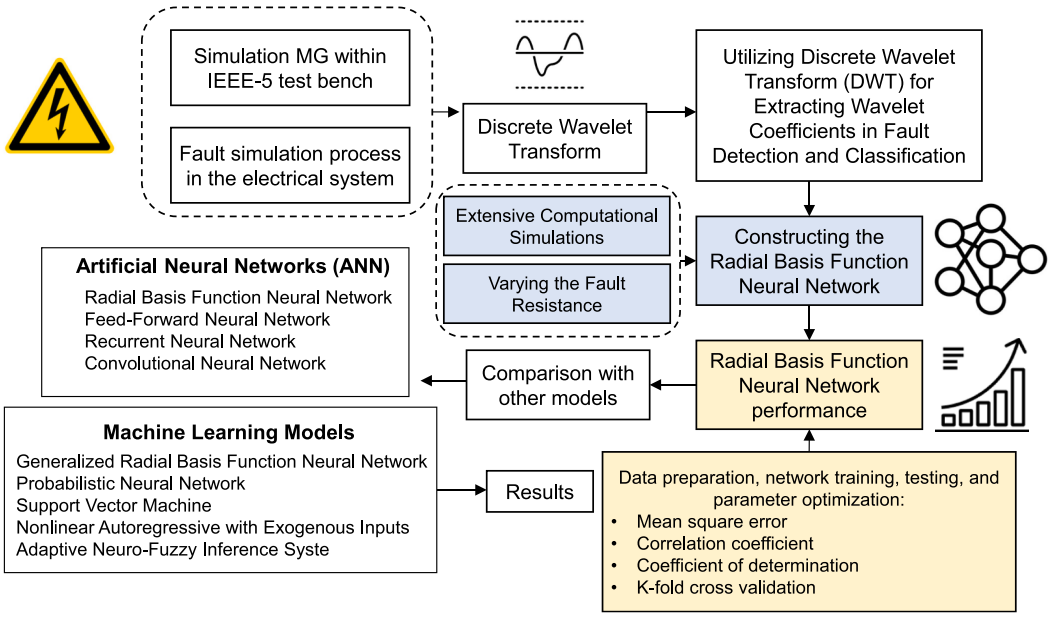

Fig. 1. Graphical representation of the proposed methodology in this study.

ring network scenario. By evaluating fault detection and classification in this context, the research aims to address the challenges posed by multiple interconnected lines, thereby contributing to a more comprehensive understanding of protection systems in microgrids.

- To bridge the research gap related to the oversight of diverse renewable sources beyond PV and WT within MGs, this work considers a renewable system comprising PV/HKT and variable load. This approach reflects the future landscape of smart grids, where various renewable sources like HKT and hybrid systems are expected. By evaluating the behavior of these diverse sources in ring network configurations during fault scenarios, this research contributes to a more inclusive understanding of microgrid protection.

The remainder of this paper is organized as follows. Section 2 outlines the proposed methodology, including the definitions of DW and RBFNN. Section 3 conducts a sensitivity analysis concerning neural network control parameters. Section 4 presents a case study, while Section 5 discusses the results and engages in comparative analysis with

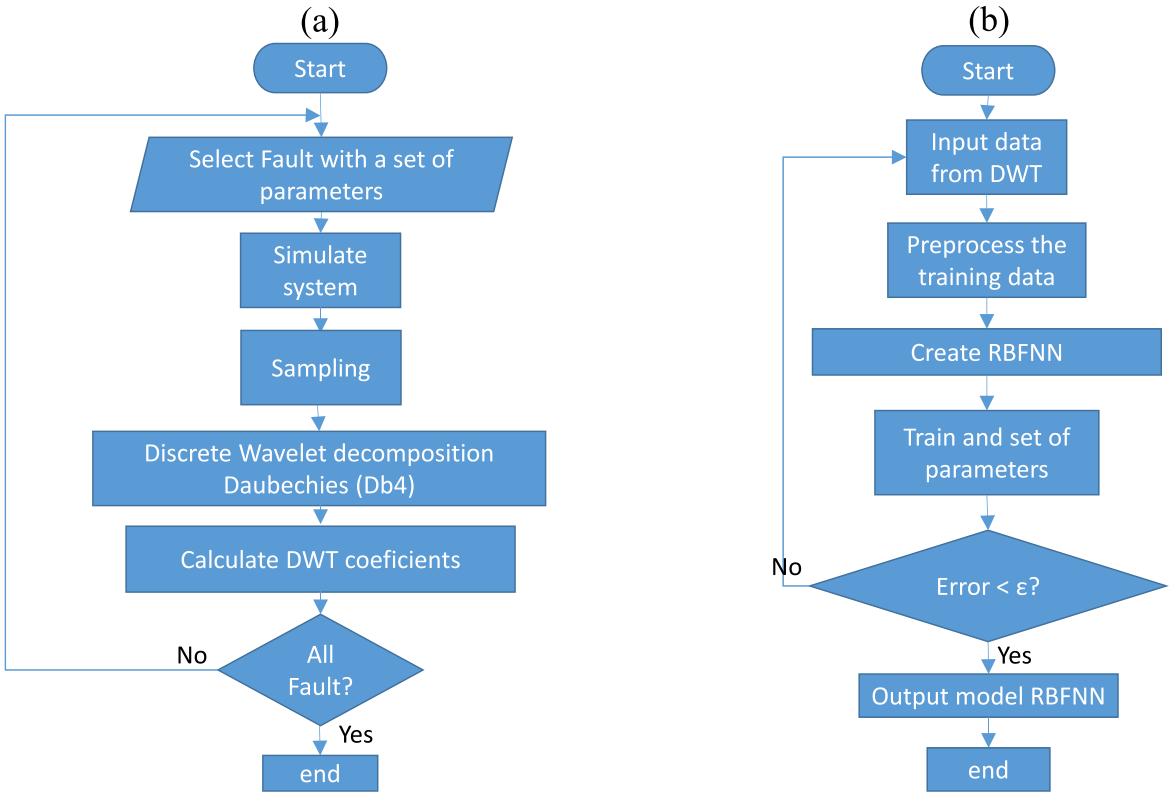

Fig. 2. Flow chart (a) DWT (b) RBFNN.

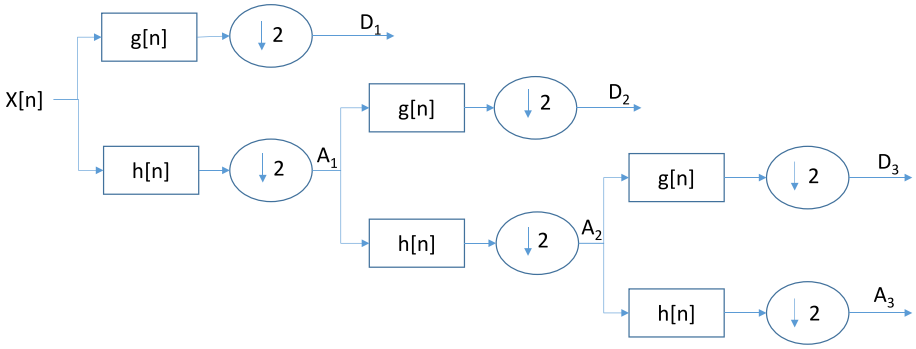

Fig. 3. Subband decomposition in the implementation of the Discrete Wavelet Transform, with g[n] representing the high-pass filter and h[n] representing the low-pass filter.

other prediction models. Finally, Section 6 provides the paper's conclusions.

2. Proposed methodology

In the proposed fault detection and classification methodology, a systematic process is employed. This process initiates with fault simulation within an IEEE-5 test bench designed to replicate real-world conditions. The initial step involves applying the DWT to fault current waveforms. This mathematical technique decomposes current waveforms into various frequency components, a critical aspect for accurate fault analysis. The outcome of this DWT analysis is the extraction of wavelet coefficients, representing crucial characteristics related to fault occurrences. These extracted wavelet coefficients are then input into a chaotic neural network, a vital component of the methodology. The chaotic neural network functions as a classifier responsible for identifying and categorizing specific faults that may occur within the MG. During this classification process, specific parameters such as fault resistance are varied to optimize DWT's performance. To ensure the robustness and reliability of the fault detection methodology, multiple computational simulations are conducted. These simulations generate a wide range of input samples, crucial for training and testing the RBFNN, a central element in the approach. By training the RBFNN with diverse data derived from simulations, its ability to make accurate fault determinations in real-world scenarios is enhanced. Finally, to validate the effectiveness of the proposed methodology, comparative analyses are conducted against powerful neural networks and machine learning techniques. The entire diagnostic process, from fault simulation to the results of fault detection and classification, is visually represented in Fig. 1, providing a clear illustration of the sequential steps involved in this innovative fault analysis approach.

More specifically, Fig. 2 illustrates the flowcharts depicting the DWT analysis process (a) and the RBFNN model (b). It is worth emphasize that obtaining the wavelet coefficients simplifies the training of the ANN. The effectiveness of the RBFNN is assessed by comparing it against an error threshold until it coverages to the optimal outcome.

2.1. Discrete wavelet transform definition

The discrete wavelet transform, is a signal processing technique that transforms a time series into a set of mutually orthogonal data points. This transformation allows for the extraction of time–frequency domain characteristics from a fault current. Wavelets, which are functions with zero mean in the time domain, are derived from a db4 mother wavelet process $\psi_{a,b}(t)$ through scaling and shifting, as defined by Eq. (1). Utilizing this relationship, the continuous wavelet transform of a signal $s(t)$ with a scale parameter a and shift parameter b is defined as in Eq. (2). The utilization of the db4 wavelet involves breaking down the traveling wave signals into distinct detail and approximation signals. These signals are subsequently integrated with data derived from the two-terminal traveling wave localization method for the purpose of fault detection. Furthermore, the DWT is obtained by discretizing the continuous wavelet transform, achieved by discretizing both the scale a and shift b, resulting in Eq. (3) by substituting the discrete values into Eq. (1), and DWT is derived by Eq. (4).

$$\psi_{a,b}(t) = \frac{1}{\sqrt{|a|}}\psi\left(\frac{t-b}{a}\right) \tag{1}$$

$$C(a,b,s(t),\psi(t)) = \int_{-\infty}^{+\infty} s(t)\psi^{*}_{a,b}(t)dt = \langle s(t),\psi_{a,b}(t)\rangle \tag{2}$$

$$\psi_{j,k}(t) = \frac{1}{\sqrt{2j}}\psi\left(\frac{t}{2j}-k\right) \tag{3}$$

$$d_{j,k} = \int_{-\infty}^{+\infty} s(t)\psi^{*}_{a,b}(t)dt = \langle s(t),\psi_{j,k}(t)\rangle \tag{4}$$

where a and b are scale and shift parameters, respectively. $\psi^{*}_{a,b}$(t) denotes the complex conjugate of $\psi_{a,b}$(t). When applied to a given signal $s(t)$, varying the scale parameter a and shift parameter b produces a family of wavelet coefficients C (a, b, $s(t)$, $\psi(t)$). Within these coefficients, $d_{j,k}$ represents the wavelet detail coefficient at level j and position k.

However, it is essential to noted that obtaining analytical solutions for wavelet coefficients is often unattainable for many signals $s(t)$. [14]. Mallet introduced a widely recognized method [23] for decomposing the signal into multiresolution levels. The multiresolution decomposition of an arbitrary signal s(t) at level M is defined by Eq. (5).

$$d_{j,k} = \sum_{k} a_{M,k}\frac{1}{\sqrt{2^M}}\varphi\left(\frac{t}{2^M}-k\right) + \sum_{j}^{M}\sum_{k} a_{M,k}\frac{1}{\sqrt{2^M}}\varphi\left(\frac{t}{2^M}-k\right) \triangleq A_M(t) + \sum_{j} D_j(t) \tag{5}$$

where $a_{M,k}$ represents the level approximation coefficients at level M, defined as $a_{M,k} = \langle s(t),\psi_{M,k}(t)\rangle$ and $\varphi(t)$ is corresponding scaling function [26]. Through this transformation, the signal $s(t)$ undergoes a decomposition process, resulting in an approximation coefficient $A_M(t)$ and a series of detail coefficients $D_j(t)$ at level M.

The use of DWT in fault detection schemes is widespread because it offers optimal resolution characteristics across various frequency ranges enhancing its feature extraction capabilities [24]. Each wavelet possesses unique characteristics in the time–frequency domain, which can influence the DWTs feature extraction effectiveness. Several wavelet families, including coif (coiflets), db (daubechies), dmey (discrete meyer), haar, bior (biorthogonal), and sym (symlets), have been employed in fault detection studies in MGs. The selection of wavelets should be strategic, considering the properties of the sampled data. In case where the data has a sufficient number of samples, the db and sym

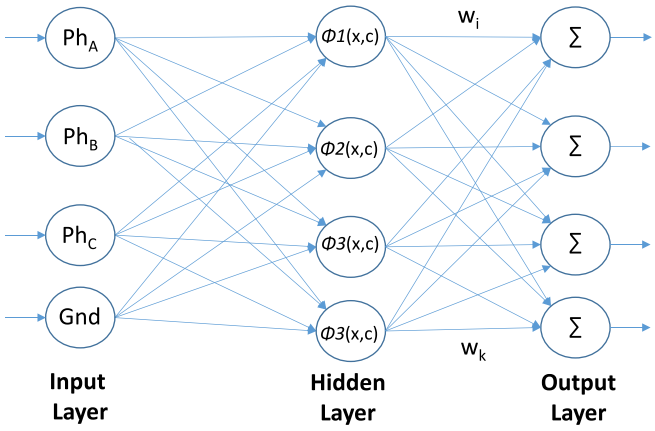

Fig. 4. Structure of RBFNN neuronal network.

wavelet families are commonly preferred due to their robustness across various data properties, including sample length. In these cases, the choice of the decomposition level M has a more significant impact on the system's performance than the specific mother wavelet selected.

In this study, we utilize four wavelets from the db family as mother wavelets to transform the input signal. In theory, each wavelet member has a maximum decomposition level, determined jointly by the input signal's size and the mother wavelet, as shown in Eq. (6).

$$L = \left\lfloor log_2 \frac{N}{F-1} \right\rfloor \tag{6}$$

The maximum decomposition level, denoted as L, is determined by both the size of the input signal N and the properties of the mother wavelet filter F [23]. Following the heuristic outlined in [24], for effective handling of current measurements, it is recommended to set the decomposition level M to its maximum value L.

The decomposition process involves multiple stages with two digital filters and downsamplers, reducing the signal by a factor of 2 at each step. The first filter, $g[\bullet]$, correspond to the discrete high-pass mother wavelet, while the second filter, $h[\bullet]$, serves as its low-passcounterpart. The high-pass filter extracts the detail component (D1), whereas the low-pass filter provides the approximation component (A1). This process iterates by further decomposing the approximation component, creating a hierarchical representation with progressively finer levels of detail (see Fig. 3).

All wavelet transforms can be represented by a low-pass filter h, satisfies the quadrature mirror condition and can be computed using Eq. (7). By applying Eqs. (8) and (9) with the initial condition $H_0(z) = 1$, a series of filters with progressively longer lengths (indexed by i) can be derived. This two-scale relationship in the time domain is expressed in Eq. (10). The normalized wavelet and scaling functions denoted as $\phi_{i,l}(k)$, $\psi_{i,l}(k)$, respectively, can be defined as shown in Eq. (11). Finally, the DWT decomposition is described by Eq. (12).

$$H(z)H\left(z^{-1}\right) + H(-z)H\left(-z^{-1}\right) = 1 \tag{7}$$

$$G(z) = zH\left(-z^{-1}\right) \tag{8}$$

$$H_{i+1}(z) = H\left(z^{2^i}\right)H_i(z), G_{i+1}(z) = G\left(z^{2^i}\right)H_i(z), i = 0, \cdots, I-1, \tag{9}$$

$$h_{i+1}(z) = [h]_{\uparrow 2^i} * h_i(k), g_{i+1}(k) = [g]_{\uparrow 2^i} * h_i(k), \tag{10}$$

$$\varphi_{i,l}(k) = 2^{i/2}h_i\left(k - 2^i l\right), \psi_{i,l}(k) = 2^{i/2}g_i\left(k - 2^i l\right), \tag{11}$$

$$a_{(i)}(l) = x(k) * \varphi_{i,l}(k), d_{(i)}(l) = x(k) * \psi_{i,l}(k), \tag{12}$$

where $H(z)$ denotes the z-transform of the filter h. The subscript $[h]_{\uparrow m}$ indicates the up-sampling by a factor of m, and k represents the discrete time samples. The factor $2^{i/2}$ is a normalization term for the inner product. The parameters i and l correspond to the scale parameter and translation parameter, respectively.

2.2. Radial basis function neural network

The RBFNN is an artificial neural network that employs radial basis functions as activation functions. It comprises three layers: a linear distribution layer, a nonlinear layer with Gaussian functions, and a linear combination layer. In the training process, the connection weights linking the hidden layer and the output layer are adjusted using the Moore-Penrose generalized pseudoinverse. The Gaussian kernel is used as the radial basis function. Fig. 4 illustrates the structure of the RBFNN.

The RBFNN offers computational efficiency and a compact topology. It excels in both global mapping generalization and local feature refinement without disrupting the existing learned mapping. The RBFNN starts with no hidden units and progressively incorporates units until a minimum radius is achieved through parameter and weight updates. Each hidden unit is characterized by center μ and width σ parameters. The hidden units in the neural network respond to the input according to Eq. (13). The output layer, which varies in size based on the types of failures being classified, performs a simple summation. The overall RBFNN output is obtained by scaling the response of each hidden unit (Eq. (7)) with its corresponding connection weights (α's) to the output nodes and summing them together Eq. (14). During the learning process of the RBFNN, new hidden units are allocated, and network parameters are adjusted. Initially, the network starts with no hidden units, and as training progresses, additional hidden units are added based on the novelty of the data. The decision to introduce a new hidden unit is determined by three conditions Eq. (15) [24]. If these conditions are met, a new hidden unit is introduced with specific parameters as defined by Eq. (16).

$$\phi_k(xx_n) = exp\left(-\frac{1}{\sigma_k^2}\|xx_n - \mu_k\|^2\right) \tag{13}$$

$$f_m(xx_n) = \alpha_{mo} + \sum_{k=1}^{K} \alpha_{mo}\phi_k(xx_n) \tag{14}$$

$$\begin{aligned} &\|xx_n - \mu_{nr}\| > \in_n \\ &e_n = |y_n - f(xx_n)| > e_{min} \\ &e_{rms} = \sqrt{\frac{\sum_{i=n-M+1} e_i^2}{M}} > e'_{min} \end{aligned} \tag{15}$$

$$\begin{aligned} &\alpha_{k+1} = e_n \\ &\mu_{k+1} = xx_n \\ &\sigma_{k+1} = \rho\|xx_n - \mu_{nr}\| \end{aligned} \tag{16}$$

where the k-th hidden unit is characterized by its central vector μ_k and width σ_k of the Gaussian function. The term $\|xx_n - \mu_k\|$ represents the Euclidean norm between the input xx_n and the central vector μ_k. K denotes the total number of hidden neurons in the RBFNN. The connection weight from the m-th hidden unit to the k-th output node is denoted as α_{mk}, and α_{m0} represents the bias term for the corresponding output neuron. The value μ_{nr} corresponds to the closest center to xx_n. The threshold values $\in_n$ represent the data window size for computing the RMS error, and $\in_n$ decays exponentially during training, indicating the resolution scale in the input space. The error thresholds e_{min} and e'_{min} represent the desired approximation accuracy of the network output. The parameter ρ represents the overlap factor.

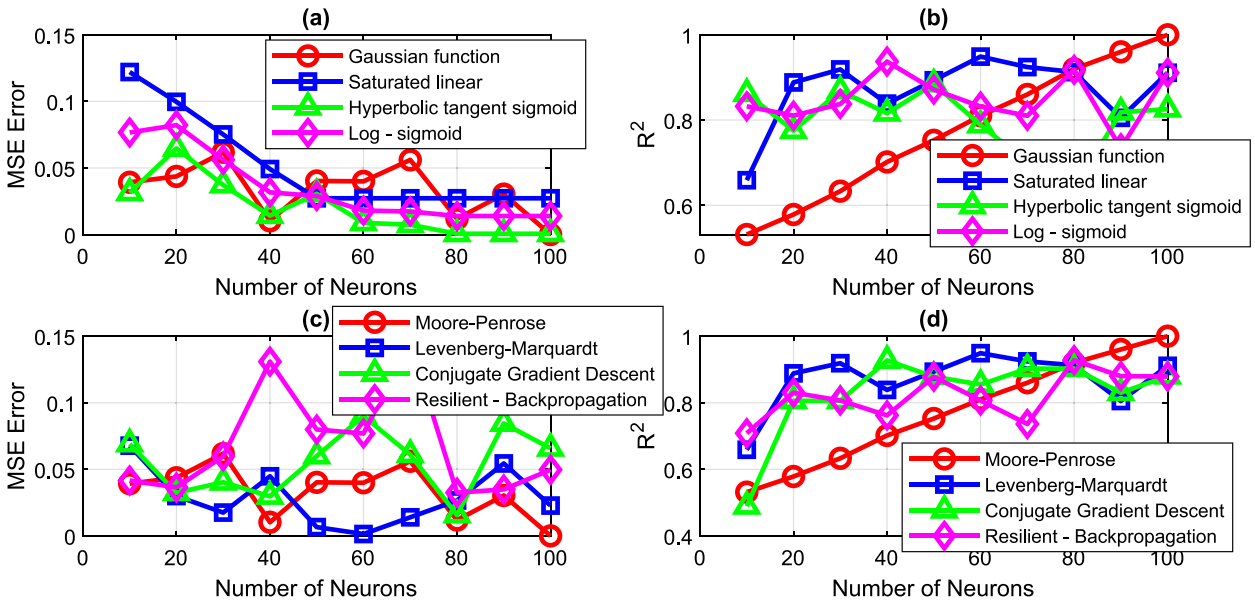

Fig. 5. Sensitivity analysis for the proposed RBFNN. (a) and (b) MSE and R^2 estimation with respect to the number of neurons different activation functions, respectively. (c) and (d) MSE and R^2 estimation with respect to the number of neurons and different training functions, respectively.

3. Analysis of sensitivity regarding neural network control parameters

This section conducts a sensitivity analysis of the proposed RBFNN neural network, exploring critical parameters to maximize its performance. Various variables were adjusted, including the number of neurons, training functions, learning rates, computational time, and activation functions, in search of the optimal configuration [25]. Specifically, when evaluating activation functions, it was observed that as the number of neurons in the hidden layer increased, the Mean Squared Error (MSE) consistently decreased for the Gaussian Radial activation function used in this study, as shown in Fig. 5 (a). In contrast, the Saturated Linear and Log-Sigmoid activation functions also exhibited a decrease in MSE as the number of neurons in the hidden layer increased, but with a shallower slope, tending to stabilize beyond 80 neurons and not reaching as low an MSE as the Gaussian Radial. However, the Hyperbolic Tangent Sigmoid function did show lower MSE values even than the Gaussian for certain numbers of neurons, but when reaching 100 neurons, the error converged to a higher value than the latter. In Fig. 5 (b), the R^2 results are presented, revealing that the Gaussian function maintains a consistently increasing trend until it reaches its maximum value, which is very close to unity, while the other activation functions exhibit variations converging to lower values. In summary, this sensitivity analysis highlights that the Gaussian Radial activation function stands out by consistently achieving a low MSE and high R^2 values, positioning it as a robust choice to enhance RBFNN performance. Although other activation functions also show promising results, the Gaussian Radial function emerges as the preferred option based on these indicators.

Regarding training algorithms, four widely recognized ones were evaluated: Moore-Penrose, Levenberg-Marquardt, Conjugate Gradient Descent, and Resilient-Backpropagation [26]. The Moore-Penrose algorithm excelled due to its consistent MSE reduction (see Fig. 5c) and impressive R^2 values (see Fig. 5d) as the number of neurons in the network increased. The Levenberg-Marquardt algorithm maintained competitive MSE and R^2 values in all neuron configurations but eventually converged to higher values than those used in this paper. On the other hand, the Conjugate Gradient and Resilient-Backpropagation algorithms exhibited variations in MSE as the number of neurons changed but consistently maintained strong R^2 values. In summary, while all evaluated algorithms proved effective, the Moore-Penrose algorithm stood out due to its impressive performance in terms of MSE and R^2, making it a promising choice for neural network applications.

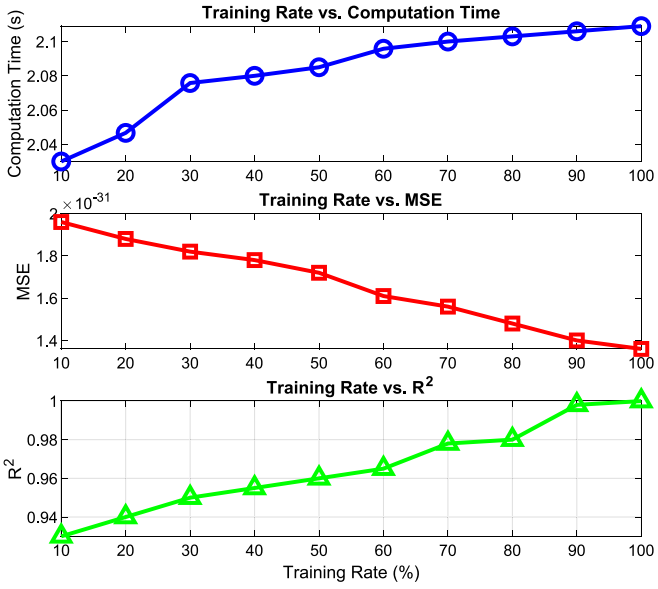

Fig. 6. Sensitivity analysis of training rate on R^2, MSE, and computation time for the proposed RBFNN.

This study also assessed the neural network's performance based on the training rate (%), examining critical aspects such as computational time, MSE, and R^2, as depicted in Fig. 6. As the trainging rate increased from 10% to 100%, significant variations in computational time were observed. The MSE consistently remained at exceptionally low levels, while the R^2 reached a peak value of 0.99994 with a learning rate of 100%.

4. Case study

This section presents the outcomes of the experimental trials conducted on the MG, which is interconnected with the IEEE 5-bus system

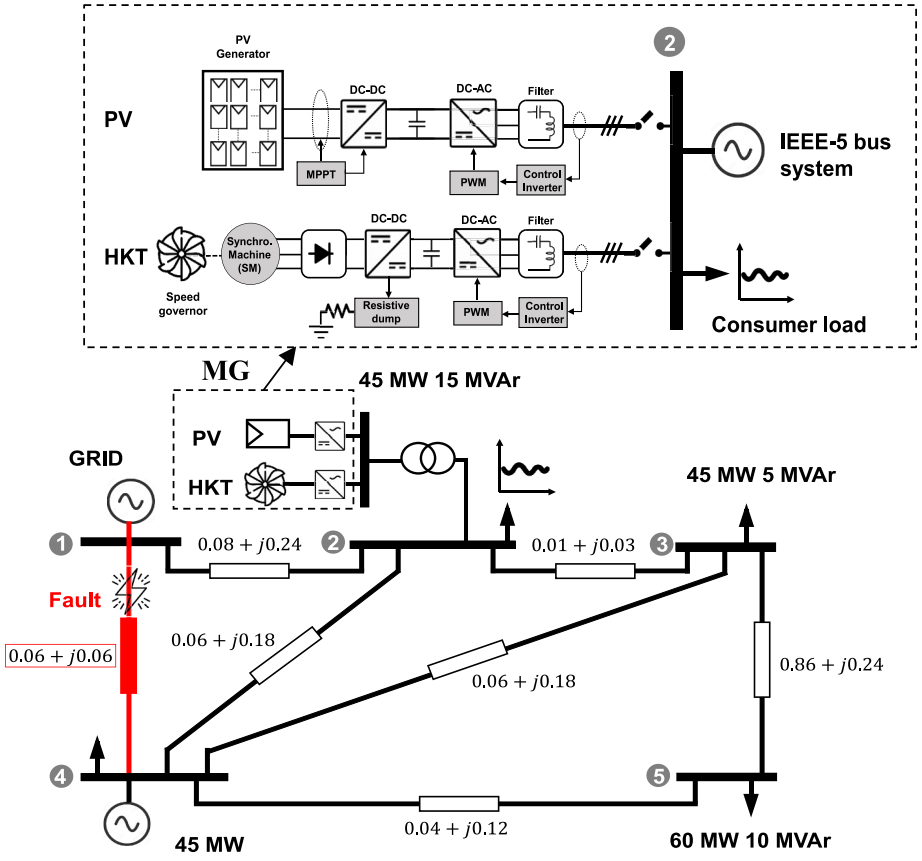

Fig. 7. IEEE-5 bus system with the connected MG.

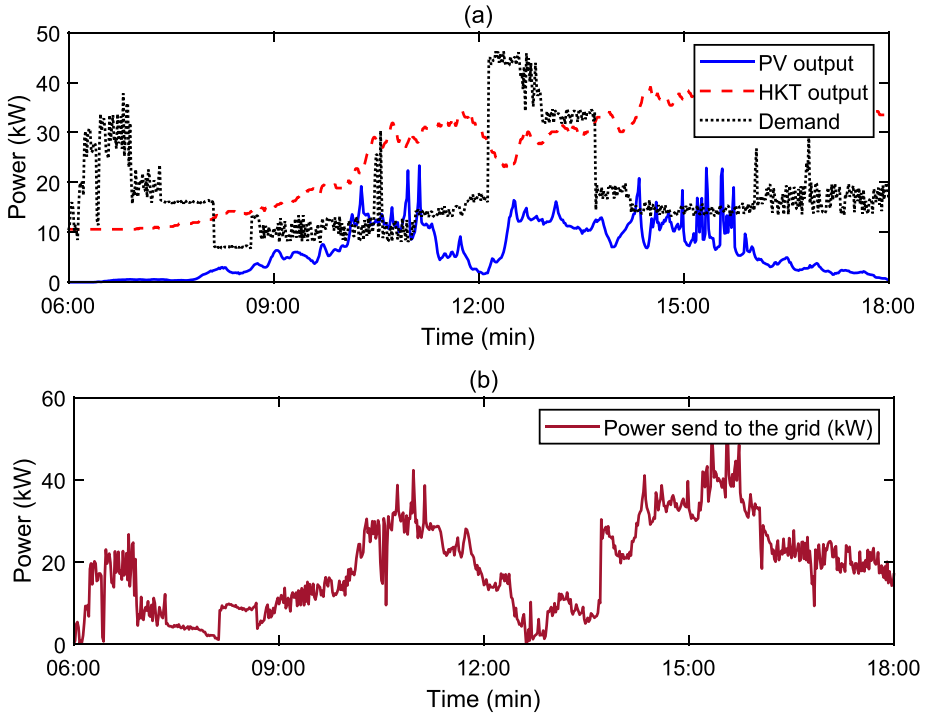

Fig. 8. Operability tests of the MG connected to IEEE-5 bus test bench. (a) Power of renewable sources and demand. (b) Power sent to the grid.

as shown in Fig. 7. The power generation profiles of each renewable source are displayed in Fig. 8. These datasets were meticulously collected from the operational MG infrastructure at the Microgrid Laboratory of the University of Cuenca [27], in addition to data from a meter-equipped residential unit. In practical implementations, several considerations regarding sampling are integral to the effectiveness of

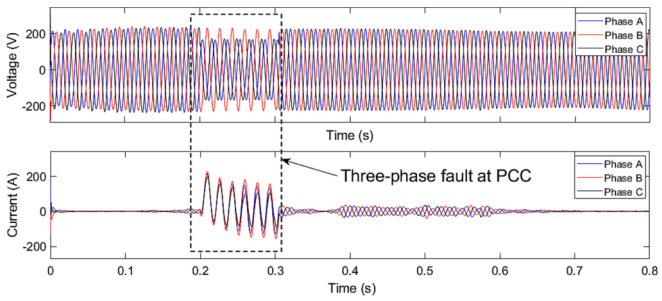

Fig. 9. System behavior during three-phase fault measured at PCC.

Table 1
Fault Case Simulation Configurations in Matlab-Simulink.

Parameter	Configuration	Count
Fault type	(A/B/C)/G, AB, AC, BC, (AB/AC/BC)/G, ABC, ABCG	12
Fault resistance	0.01 – 100 Ohm	144

our methodology in real-world scenarios. The energy control algorithm used in this study prioritizes the utilization of renewable energy sources to meet the load requirements, reducing reliance on the grid. Excess electricity generated by the MG is seamlessly fed into the grid, as illustrated in Fig. 8 (b). Extensive simulations and meticulous fault scenarios were executed within the MG system to determine the optimal operational point aligning with the specific objectives of this investigation. Furthermore, to enhance fault detection and classifications capabilities, the originally time window, despicting in Fig. 7, which covered a 12-hour daily duration, was substantially reduced to a high-resolution sampling of 0.4 s. This adjustment enables precise identification of fault occurrences within the MG system.

Strategically placing sensors within the MG, optimizing data acquisition timing, conducting thorough data preprocessing, implementing redundancy measures, and addressing data storage and transmission issues are critical aspects that demand meticulous attention in practical implementations. These considerations collectively reinforce the robustness and reliability of the methodology when applied in real-world MG scenarios connected to larger systems. By incorporating these sampling-related considerations into the experimental setup, we align the fault detection and classification process with the specific requirements and characteristics of the microgrid, thereby enhancing the practical applicability of our findings.

A three-phase fault was simulated between buses 1 and 4 of the configuration. This simulation was conducted to obtain clearer readings of the essential parameters required for building the ANN. After the fault occurred, current and voltage values were measured at the point of common coupling (PCC), and the results are depicted in Fig. 9. The system's response to a three-phase fault is shown, characterized by a decay in voltage and a corresponding surge in. This surge can be attributed to contributions from both the main generator and the PV/HKT generators within the MG. For this specific test, a sampling rate of 0.8 s was employed.

Multiple simulations were conducted to evaluate the performance of the proposed fault detection scheme. These simulations involved various fault types categorized by different ground resistance levels and other parameters, as outlined in Table 1. Measurements were taken at multiple locations whitin the system to account for potential noise-related issues and determine the optimal measurement point between bus 1 and bus 2. It's important to highlight that these simulations were executed using a Matlab-Simulink-based model that includes the MG within the IEEE-5 bus test system. Comprehensive fault scenarios and measurements were performed across different network configurations, including radial and loop modes, as well as connected and isolated modes. This was done to test the model's robustness and generalizability. The computational calculations were carried out on an Intel Core i7-10700 CPU operating at a frequency of 2.90 GHz, and the time series simulations were implemented using Matlab-Simulink. As a result, Fig. 10 illustrates the conditions of three-phase fault currents, both before and after simulation, between bus 1 and bus 2.

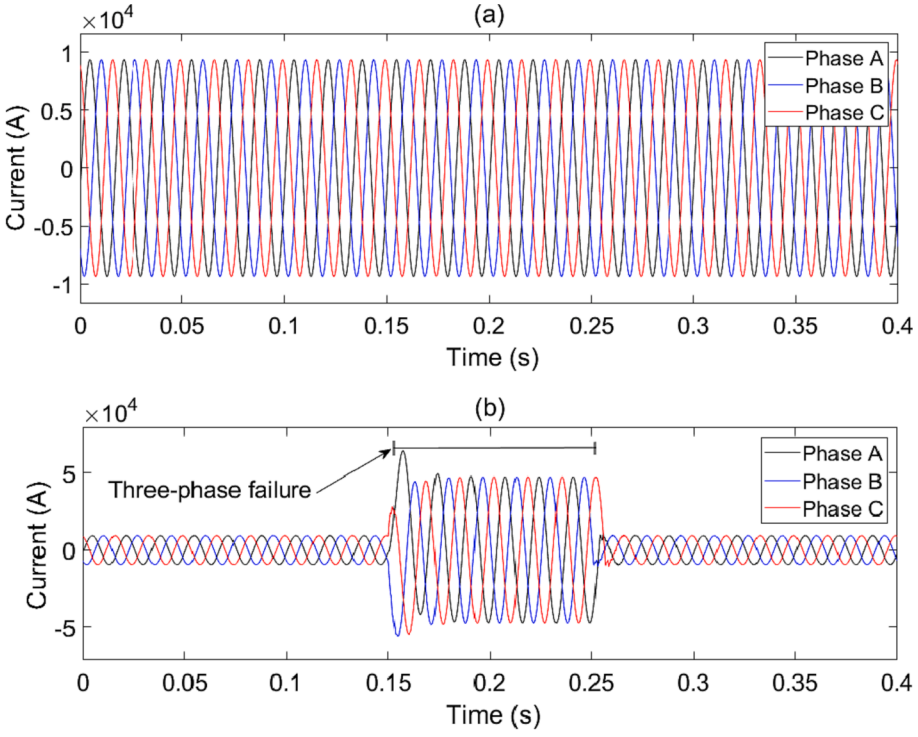

Fig. 10. Simulation of a three-phase fault in the IEEE-5 bus and MG system. (a) Three-phase alternating current representation before the fault. (b) Three-phase alternating current representation during the fault.

Table 2
Coefficient determination results for wavelet with various fault resistance.

No.	Fault Ground Resistance	Type of Fault	Max. Coefficient of Phase A	Max. Coefficient of Phase B	Max. Coefficient of Phase C	Max. Coefficient of Ground Current
1	R = 0.01	ABC-G	66.894	60.406	60.360	0.172
2	R = 0.01	ABC	66.894	60.406	61.891	0
3	R = 0.01	AB-G	64.696	61.217	13.779	0.17
4	R = 0.01	AC-G	58.852	10.402	55.686	0.152
5	R = 0.01	BC-G	14.785	77.130	70.490	0.128
6	R = 0.01	A-B	58.630	46.342	12.563	0
7	R = 0.01	A-C	45.846	13.224	72.337	0
8	R = 0.01	B-C	15.874	60.981	54.253	0
9	R = 0.01	A-G	61.009	13.658	13.631	0.213
10	R = 0.01	B-G	12.795	65.500	12.563	0.174
11	R = 0.01	C-G	13.554	12.074	67.843	0.188
12	R = 0.01	No	11.836	12.283	13.008	0
13	R = 1	ABC-G	66.894	60.406	60.360	0.0237
14	R = 1	ABC	66.894	60.406	61.891	1.14E-07
15	R = 1	AB-G	60.234	53.170	12.563	0.0146
16	R = 1	AC-G	45.935	12.149	61.622	0.0124
17	R = 1	BC-G	12.745	78.267	69.487	0.0107
18	R = 1	A-B	58.630	46.342	12.563	1.7E-08
19	R = 1	A-C	45.846	13.224	72.337	1.7E-08
20	R = 1	B-C	15.874	60.981	54.253	1.4E-08
21	R = 1	A-G	17.027	11.265	12.563	0.0204
22	R = 1	B-G	14.704	22.965	12.563	0.0294
23	R = 1	C-G	13.035	11.266	19.826	0.0231
24	R = 1	No	12.878	12.283	13.008	0
25	R = 10	ABC-G	66.894	60.406	64.294	0.0085
26	R = 10	ABC	66.894	60.406	61.891	0.00000014
27	R = 10	AB-G	58.056	46.102	12.563	0.0013
28	R = 10	AC-G	60.511	14.461	66.068	0.0017
29	R = 10	BC-G	15.420	70.225	68.445	0.0015
30	R = 10	A-B	58.630	46.342	12.563	1.4E-08
31	R = 10	A-C	45.846	13.224	72.337	1.4E-08
32	R = 10	B-C	15.874	60.981	54.253	1.4E-08
33	R = 10	A-G	12.945	13.451	12.563	0.0025
34	R = 10	B-G	15.751	13.069	13.051	0.003
35	R = 10	C-G	12.336	15.427	14.432	0.0096
36	R = 10	No	12.878	12.283	13.008	0
.....						
133	R = 100	ABC-G	66.894	60.406	62.406	0.00114342
134	R = 100	ABC	66.894	60.406	61.891	1.1488E-07
135	R = 100	AB-G	58.736	52.926	15.703	0.00016694
136	R = 100	AC-G	44.672	13.061	70.591	0.00019713
137	R = 100	BC-G	15.768	60.446	62.986	0.00014983
138	R = 100	A-B	58.630	46.341	12.563	1.271E-08
139	R = 100	A-C	45.846	13.224	72.337	1.2983E-08
140	R = 100	B-C	15.874	60.981	54.253	1.4653E-06
141	R = 100	A-G	12.922	12.694	12.563	0.00023446
142	R = 100	B-G	11.923	12.482	13.042	0.00040962
143	R = 100	C-G	12.533	11.820	12.563	0.0007002
144	R = 100	No	58.630	463.415	12.563	1.271E-08

5. Results and discussions

To obtain the results from the RBFNN, it is imperative to collect training data. In this case, this data consist of the wavelet coefficients corresponding to each type of fault. We conducted a comprehensive set of 144 simulations, covering various fault types and ground resistances. The results of the initial 12 simulations, comprising 12 values for each resistance value (R = 0.01, 1, 10, and 100 O), are presented in Table 2. However, for brevity and to conserve space, specific values (ranging from 20 to 90 O) are omitted from this Table 2. It's important to note that these omitted values are still included in the subsequent neural network analyses. This data is generated through a signal discretization followed by the computation of the peak db4 coefficient within the sample. Fig. 11 illustrates the detailed procedure used to determine the coefficient related to Phase A in the fault current.

After establishing the coefficients for all 144 potential scenarios, they are designated as input data for the RBFNN. The output data, shown in Table 3, is binary, indicating the presence (1) or absence (0) of a fault. A subset of the 144 data points is presented due to space constraint.

In ths paper, a robust normalization technique called min–max scaling was employed to normalize the input data for the RBFNN [28]. The input dataset consists of 144 real numbers, while the output dataset comprises 144 binary numbers. To ensure consistent and unbiased training of the RBFNN, the input data underwent the min–max scaling procedure. This technique transforms the input values to a standardized range, typically between 0 and 1, by utilizing the minimum and maximum values observed within the original dataset.

The normalization process is carried out using the Eq. (17):

$$X_{norm} = (X - X_{min})/(X_{max} - X_{min}) \tag{17}$$

where X represents the original data value, X_{min} denotes the minimum value observed within the dataset, X_{max} is the maximum value observed within the dataset and X_{norm} indicates the normalized value of the data.

By employing this technique, all input data is standardized within a consistent range, allowing for the efficient training of the RBFNN. This approach ensures that no single input variable dominates the learning process due to its magnitude compared to others. Additionally, it is important to note that 70% of the dataset was used for training the

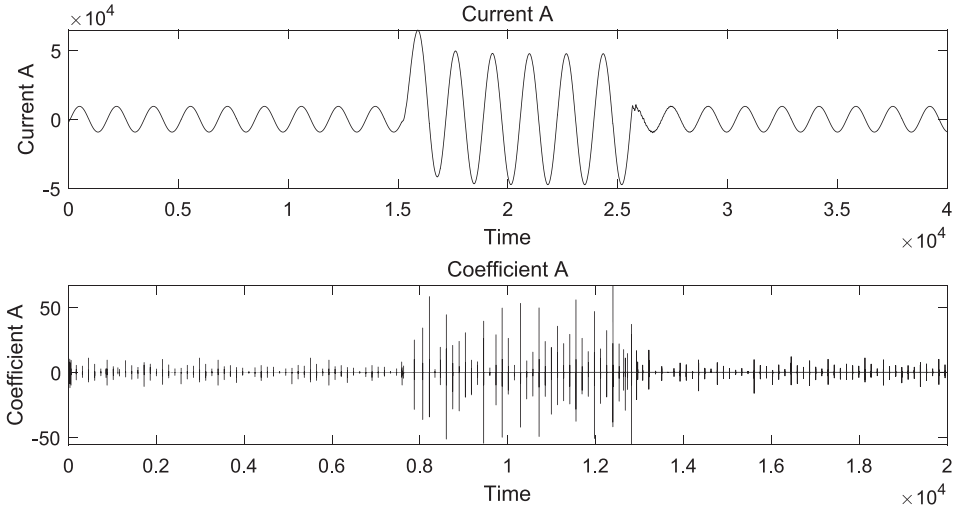

Fig. 11. Wavelet coefficient determination in phase A during the fault.

RBFNN, while the remaining 30% was allocated for testing its performance and generalization capabilities. Retaining the normalization range (minimum and maximum values) is crucial to revert the normalized results obtained from the RBFNN back to their original scale if necessary, for the purpose of result presentation or further analysis. These procedures ensure the reliability and reproducibility of the training and testing phases, facilitating the interpretation and evaluation of the RBFNN's performance in relation to the given problem statement.

As a result, Table 4 presents the outcomes for a randomly selected subset of outputs, demostrating a high level of accuracy.

The achieved performance level of $1.31e^{-31}$ is truly remarkable, especially considering the nature of the input data and the binary output that represents fault or non-fault conditions. The RBFNN's ability to attain such an exceptionally low error demonstrates its capability to accurately classify and predict fault conditions based on these intricate input patterns. Fig. 12 provides a graphical representation of the correlation between the predicted outputs and the ground truth values, clearly showcasing the network's precise classification accuracy in identifying fault occurrences. The consistent and high level of accuracy achieved by RBFNN highlights its effectiveness as a powerful tool for fault detection in complex electrical systems, demonstrating its potential for practical applications and its contribution to improving system reliability and performance.

The linear regression analysis of the RBFNN provides insights into the relationship between the predicted outputs and the actual target values. It quantitative measures how closely the RBFNN's predictions align with the ground truth. Fig. 13 displays the precision and validation results of the RBFNN model. The validation process yields an impressive correlation coefficient (R) of 0.99994, indicating a strong linear relationship between the predicted and actual values. Similarly, the coefficient of determination (R^2) for the overall performance of the RBFNN is 0.99998, signifying that the model captures a substantial portion of the variance in the data and demostrates an outstanding level of accuracy and reliability. These high correlation coefficients underscore the robustness and effectiveness of the RBFNN in precisely predicting the target values.

After completing the validation of the neural network through conventional testing, an additional evaluation was carried out using K-fold cross-validation with K = 15 to confirm its performance in fault detection and classification [29]. The results of this evaluation are presented in Fig. 14 and are highly promising. A consistently low MSE and a high coefficient of determination R^2 are observed, indicating the accuracy of predictions made by the RBFNN in fault detection scenarios.

5.1. Comparative with other prediction models

To evaluate the effectiveness of the RBFNN method, it's essential to compare it with other prediction models, including a machine learning technique and various ANNs. The GRNN, which utilizes radial basis functions for data prediction, bears some similarities to the RBFNN. However, there's a scarcity of research combining DWT with fault prediction or classification in electrical systems, although DWT has been explored in other applications like electricity demand prediction [30], wind energy prediction [31], and transmission line outage prediction [32]. Other ANN models, such as PNN and FFNN, which operate on a direct feed principle, are also considered for comparison. Previous research has examined the use of DWT and PNN for fault detection in transmission lines. Feedforward models have shown promising results in DWT signal analysis [33], especially in MGs with renewable sources [34]. Additionally, various ANN models, such as Recurrent Neural Network (RNN) or Nonlinear Autoregressive with External Input (NARX), have been considered [35]. Machine learning models like Convolutional Neural Network (CNN) [36] and Support Vector Machine (SVM) have shown excellent performance in fault detection [37]. A line-by-line fault detection method in PV arrays using SVM has been proposed for systems with renewable sources [38]. The Adaptive Neuro-Fuzzy Inference System (ANFIS) has also been employed in fault detection techniques [39]. Adjusting the optimization function is necessary in some cases [40].

It's important to recognize that the choice of a specific model depend on the nature of the problem, data availability, and the specific accuracy and performance requirements. Therefore, in this paper, the aforementioned ANN and machine learning models have been customized to yield optimal outcomes in each specific case. For ANN, iterative algorithms have been developed to determine the optimal solution by considering factor such as the number of epochs, the quantity of hidden layers, the MSE, and the computational time. Conversely, SVM has demonstrated superior convergence performance by using parameters like Coding = onevsall and Kernel function = Linear. The number of hidden layers has been set at 10 to establish a comparative reference framework.

The number of epochs at which the function converges has been selected, and two ANFIS membership function has been employed, as increasing this parameter renders the computational time impractical. The comparative results are presented in Table 5.

One of the primary challenges in this comparative analysis has been fine-tuning each method to match the specific input and output variables. The results indicate that both RBFNN and GRNN exhibit exceptional capabilities in modeling complex nonlinear relationships,

Table 3
Defined outputs for RBFNN based on wavelet coefficients.

No.	Fault Ground Resistance	Type of Fault	Max. coefficient of Phase A	Max. coefficient of Phase B	Max. coefficient of Phase C	Max. coefficient of Ground Current
1	R = 0.01	ABC-G	1	1	1	1
2	R = 0.01	ABC	1	1	1	0
3	R = 0.01	AB-G	1	1	0	1
4	R = 0.01	AC-G	1	0	1	1
5	R = 0.01	BC-G	0	1	1	1
6	R = 0.01	A-B	1	1	0	0
7	R = 0.01	A-C	1	0	1	0
8	R = 0.01	B-C	0	1	1	0
9	R = 0.01	A-G	1	0	0	1
10	R = 0.01	B-G	0	1	0	1
11	R = 0.01	C-G	0	0	1	1
12	R = 0.01	No	0	0	0	0
13	R = 1	ABC-G	1	1	1	1
14	R = 1	ABC	1	1	1	0
15	R = 1	AB-G	1	1	0	1
16	R = 1	AC-G	1	0	1	1
17	R = 1	BC-G	0	1	1	1
18	R = 1	A-B	1	1	0	0
19	R = 1	A-C	1	0	1	0
20	R = 1	B-C	0	1	1	0
21	R = 1	A-G	1	0	0	1
22	R = 1	B-G	0	1	0	1
23	R = 1	C-G	0	0	1	1
24	R = 1	No	0	0	0	0
25	R = 10	ABC-G	1	1	1	1
26	R = 10	ABC	1	1	1	0
27	R = 10	AB-G	1	1	0	1
28	R = 10	AC-G	1	0	1	1
29	R = 10	BC-G	0	1	1	1
30	R = 10	A-B	1	1	0	0
31	R = 10	A-C	1	0	1	0
32	R = 10	B-C	0	1	1	0
33	R = 10	A-G	1	0	0	1
34	R = 10	B-G	0	1	0	1
35	R = 10	C-G	0	0	1	1
36	R = 10	No	0	0	0	0
.....						
133	R = 100	ABC-G	1	1	1	1
134	R = 100	ABC	1	1	1	0
135	R = 100	AB-G	1	1	0	1
136	R = 100	AC-G	1	0	1	1
137	R = 100	BC-G	0	1	1	1
138	R = 100	A-B	1	1	0	0
139	R = 100	A-C	1	0	1	0
140	R = 100	B-C	0	1	1	0
141	R = 100	A-G	1	0	0	1
142	R = 100	B-G	0	1	0	1
143	R = 100	C-G	0	0	1	1
144	R = 100	No	0	0	0	0

demostrating remarkable performance in function approximation problems, rapid learning, and the ability to effectively model sequential time-series data and previous states. Consequently, these models show the lowest MSE and, thus, the highest overall performance. It's important to note that while RBFNN requires fewer epochs to converge to an optimal solution, its training time is significantly longer due to the inherent difficulties associated with training on lengthy sequences, such as the vanishing or exploding gradient problems.

Moving forward, SVM stands out as a top performer due to its efficacy in handling high-dimensional datasets, showing excellent performance in both linear and nonlinear classification tasks, and its resilience against overfitting. Consequently, SVM exhibits the most favorable training time, providing an optimal balance between computational effort and performance. However, it's worth mentioning that SVM may requiere careful selection of hyperparameters and can eface challenges when dealing with imbalanced datasets. The results for NARX are also commendable, with low computational time and convergence achieved with a relatively small number of epochs. Its superior performance makes it a promising candidate for this type of problem, albeit requiring meticulous parameter tuning. On the other hand, ANFIS has the advantage of modeling intricate relationships by leveraging the synergy between fuzzy logic and ANNs, enabling automatic learning of inference rules. This characteristic proves especially powerful in scenarios characterized by high variability. However, ANFIS involves determining initial rules and fuzzy sets, resulting in a considerably longer training time compared to other methods. In fact, increasing the membership function to three leads to a quadrupling of the training time.

Lastly, PNN, FFNN, and CNN exhibit lower precision but excel in terms of training time and number of epochs. This outcome can be attributed to several factors, including CNN's reliance on substantial amounts of unstructured training data to achieve optimal performance, PNN's sensitivity to redundant input data, and FFNN's lack of memory of previous states.

In summary, the evaluated models offer distinct advantages that can be leveraged for fault detection and classification in renewable MG power systems. While all methods yield excellent results, it is important to consider factors such as training time, accuracy, and simplicity. In this context, RBFNN emerges as the most suitable option for the problem presented in this research endeavor.

Table 4
RBFNN predictive results for fault detection and classification.

RBFNN Forecasting				Real data			
1	1	1	1	1	1	1	1
1	1	1	−4.58E−08	1	1	1	0
1	1	4.08E−12	1	1	1	0	1
1	−8.73E−12	1	0.99999999	1	0	1	1
8.76E−12	1	1	1.00000005	0	1	1	1
1	1	−3.23E−12	3.68E−09	1	1	0	0
1	−3.63E−09	1	1.99E−07	1	0	1	0
3.12E−09	1	1	−9.68E−06	0	1	1	0
1	−7.25E−12	1.36E−11	0.99999999	1	0	0	1
−8.29E−12	1	1.63E−11	0.99999999	0	1	0	1
−7.14E−12	−8.10E−12	1	0.99999999	0	0	1	1
2.64E−10	9.92E−10	−1.19E−10	−8.67E−09	0	0	0	0
1	1	1	0.99999999	1	1	1	1
1	1	1	−3.46E−09	1	1	1	0
1	1	−7.77E−13	1	1	1	0	1
1	−1.07E−11	1	0.99999999	1	0	1	1
2.33E−11	1	1	1	0	1	1	1
1	1	2.41E−12	−7.73E−10	1	1	0	0
1	−1.09E−11	1	−1.00E−08	1	0	1	0
3.79E−11	1	1	−3.99E−08	0	1	1	0
1	−7.25E−12	1.36E−11	0.99999999	1	0	0	1
−8.29E−12	1	1.63E−11	0.99999999	0	1	0	1
−7.14E−12	−8.10E−12	1	0.99999999	0	0	1	1
2.64E−10	9.92E−10	−1.19E−10	−8.67E−09	0	0	0	0
1	1	1	1	1	1	1	1
1	1	1	2.96E−08	1	1	1	0
1	1	4.52E−13	1	1	1	0	1
1	−1.27E−11	1	0.99999999	1	0	1	1
1.48E−12	1	1	0.99999999	0	1	1	1
1	1	5.94E−12	−3.17E−09	1	1	0	0
1	−3.63E−09	1	1.99E−07	1	0	1	0
−1.16E−09	1	1	3.73E−06	0	1	1	0
1	−7.25E−12	1.36E−11	0.99999999	1	0	0	1
−8.29E−12	1	1.63E−11	0.99999999	0	1	0	1
−7.14E−12	−8.10E−12	1	0.99999999	0	0	1	1
−1.77E−09	−6.47E−09	9.36E−10	9.98E−09	0	0	0	0
0.99971929	0.99766875	1.00233144	0.45245604	1	1	1	1
1	1	1	2.96E−08	1	1	1	0
1.00004176	0.99663426	0.00083	0.62644936	1	1	0	1
0.99995929	0.00717267	0.99550	1.2852454	1	0	1	1
0.00824721	1.00709398	0.99115	4.87969207	0	1	1	1
1	1	−3.23E−12	3.68E−09	1	1	0	0
1	−3.63E−09	1	1.99E−07	1	0	1	0
−1.16E−09	1	1	3.72E−06	0	1	1	0
1	−7.25E−12	1.36E−11	0.99999999	1	0	0	1
−8.29E−12	1	1.63E−11	0.99999999	0	1	0	1
−7.14E−12	−8.10E−12	1	0.99999999	0	0	1	1
−1.77E−09	−6.47E−09	9.36E−10	9.98E−09	0	0	0	0

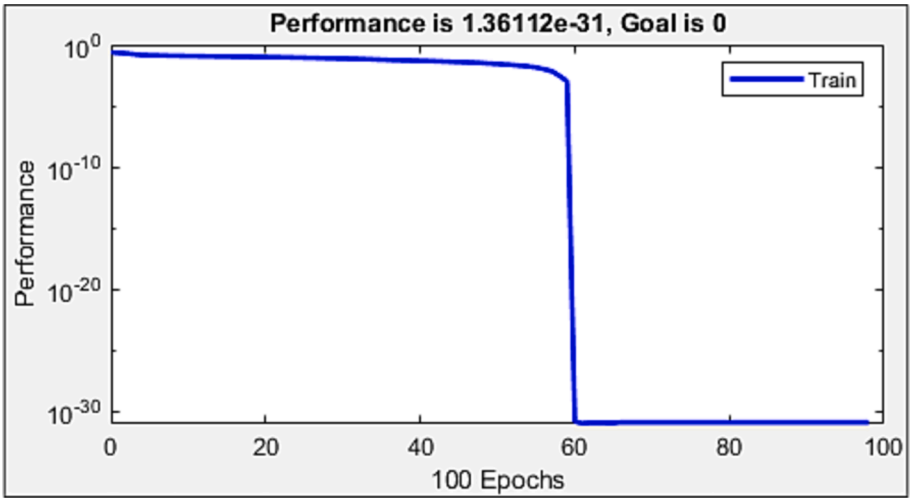

Fig. 12. Performance evaluation of prediction error analysis of the RBFNN model.

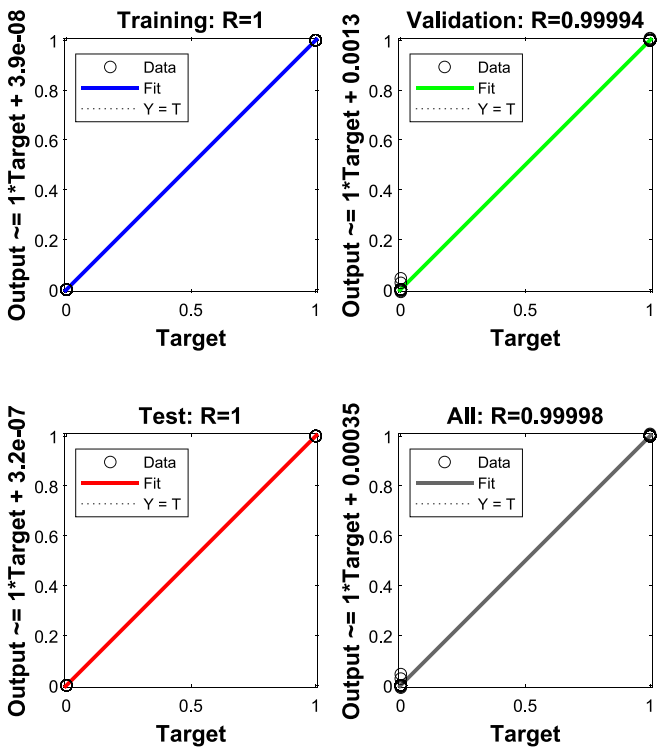

Fig. 13. Validation results of RBFNN using regression analysis.

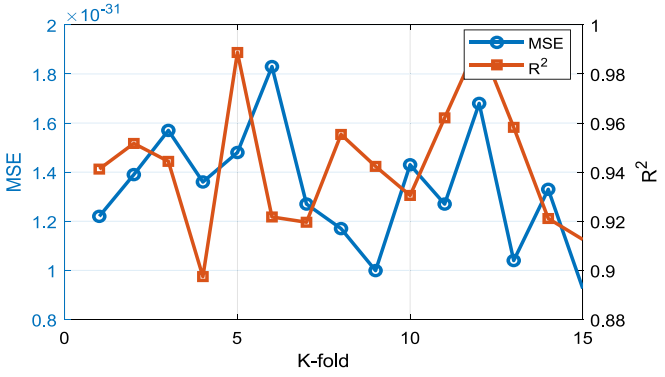

Fig. 14. MSE and R^2 results using K-fold cross-validation.

6. Conclusions

This paper presents an innovative methodology for fault detection and classification in renewable microgrids, addressing the unique challenges posed by bidirectional energy flow and nonlinear relationships within these systems. The main conclusions of our research are as follows: the integration of the discrete wavelet transform with various neural network models enhances accuracy in fault detection, especially in scenarios involving nonlinear elements such as photovoltaic, hydrokinetic, and variable electric load systems. The radial basis function neural network model demonstrates outstanding accuracy, with a minimum error of 1.31e-31. In a comparative analysis, the radial basis function neural network and generalized radial basis function neural network models show superior accuracy and performance. Support vector machines excel in handling high-dimensional datasets, while nonlinear autoregressive with exogenous inputs models show noteworthy results with low computational time. The adaptive neuro-fuzzy inference system proves effective in modeling complex relationships but requires longer training times. Models like probabilistic neural network, feed-forward neural network, and convolutional neural network offer simplicity and quick training, albeit with lower precision. In summary, this research provides a robust fault detection methodology specifically tailored to renewable energy microgrids, offering improved accuracy and performance, ultimately contributing to the reliability of renewable energy integration into the electrical grid. The radial basis function neural network model stands out as a powerful tool for fault detection in these systems. It's worth noting that in this study, ground resistance was varied, with high values (up to 100 O), and faults were correctly identified even under high ground resistance conditions, demonstrating the robustness of the proposed methodology. However, it's worth noting that the study primarily focuses on addressing low- and medium-impedance faults, which were relevant to the current research objectives. While the exclusion of high-impedance faults is not considered a substantial limitation in the context of this study, it does offer opportunities for future research endeavors. In future work, we plan to explore the comprehensive analysis of high-impedance faults in microgrids, which will contribute to further enhancing the reliability of these systems.

Table 5
Fault detection results using DWT-based prediction - comparative analysis of ANN and machine learning models.

Model	MSE	Time of training (s)	Epoch of best performance	Hidden Layers
RBFNN	1.31E−31	1.63	100	10
GRNN	6.87E−05	1.66	50	10
PNN	0.23	0.49	20	10
FFNN	0.03	0.56	8	10
RNN	3.27E−27	4.49	12	10
NARX	6.35E−11	0.59	59	10
CNN	0.46	0.86	46	10
SVM	3.00E−23	0.017	Coding = onevsall	Kernel function = Linear
ANFIS	1.25E−05	4.98	10	Membership Function = 2

Declaration of Competing Interest

The authors declare that they have no known competing financial interests or personal relationships that could have appeared to influence the work reported in this paper.

Data availability

Data will be made available on request.

Acknowledgment

The author (Paul Arévalo) thanks the Call for Grants for the Requalification of the Spanish University System for 2021-2023, Margarita Salas Grants for the training of young doctors awarded by the Ministry of Universities and financed by the European Union –Next Generation EU.

The author Dario Benavides is grateful for a Doctoral Training Program in the area of Engineering and Technical Sciences (UMA, Spain; UTI, UTM, UTN, Ecuador) of Asociación Universitaria Iberoamericana de Postgrado (AUIP).

The icons used in this document were developed by Freepik, monkik, Smashicons and Pixel perfect, from www.flaticon.com.

The authors acknowledge the support provided by the Thematic Network 723RT0150 "Red para la integración a gran escala de energías renovables en sistemas eléctricos (RIBIERSE-CYTED)'' financed by the call for Thematic Networks of the CYTED (Ibero-American Program of Science and Technology for Development) for 2022.

References

[1] Coelho A, Neyestani N, Soares F, Lopes JP. Wind variability mitigation using multi-energy systems. Int J Electr Power Energy Syst 2020;118:105755. https://doi.org/10.1016/J.IJEPES.2019.105755.

[2] Patnaik B, Mishra M, Bansal RC, Jena RK. AC microgrid protection – A review: Current and future prospective. Appl Energy 2020;271:115210. https://doi.org/10.1016/J.APENERGY.2020.115210.

[3] Ali Dashtaki A, Mehdi Hakimi S, Hasankhani A, Derakhshani G, Abdi B. Optimal management algorithm of microgrid connected to the distribution network considering renewable energy system uncertainties. Int J Electr Power Energy Syst 2023;145:108633. https://doi.org/10.1016/J.IJEPES.2022.108633.

[4] Mandintereza PT, Bansal RC. Review of technical issues influencing the decoupling of DG converter design from the distribution system protection strategy. IET Renew Power Gener 2018;12:1091–100. https://doi.org/10.1049/IET-RPG.2017.0670.

[5] Mandintereza PT, Bansal R. Renewable distributed generation: The hidden challenges – A review from the protection perspective. Renew Sustain Energy Rev 2016;58:1457–65. https://doi.org/10.1016/J.RSER.2015.12.276.

[6] Raza A, Benrabah A, Alquthami T, Akmal M. A Review of Fault Diagnosing Methods in Power Transmission Systems. Appl Sci 2020;10:1312. https://doi.org/10.3390/APP10041312.

[7] Muniappan M. A comprehensive review of DC fault protection methods in HVDC transmission systems. Protection Control Modern Power Syst 2021;6:1–20. https://doi.org/10.1186/S41601-020-00173-9/FIGURES/16.

[8] Zarif M, Miranian A. Model predictive control of multi-terminal DC grids with offshore wind farms. In: 3rd International Conference on Renewable Energy Research and Applications, (ICRERA 2014). p. 717–21.

[9] Montoya R, Poudel BP, Bidram A, Reno MJ. DC microgrid fault detection using multiresolution analysis of traveling waves. Int J Electr Power Energy Syst 2022;135:107590. https://doi.org/10.1016/J.IJEPES.2021.107590.

[10] Gogula V, Edward B. Fault detection in a distribution network using a combination of a discrete wavelet transform and a neural Network's radial basis function algorithm to detect high-impedance faults. Front Energy Res 2023;11:1101049. https://doi.org/10.3389/FENRG.2023.1101049/BIBTEX.

[11] Chen X, Gao W, Hong C, Tu Y. A novel series arc fault detection method for photovoltaic system based on multi-input neural network. Int J Electr Power Energy Syst 2022;140:108018. https://doi.org/10.1016/J.IJEPES.2022.108018.

[12] Allal A, Khechekhouche A. Diagnosis of induction motor faults using the motor current normalized residual harmonic analysis method. Int J Electr Power Energy Syst 2022;141:108219. https://doi.org/10.1016/J.IJEPES.2022.108219.

[13] Li D, Ukil A. Fault detection method using high-pass filtering in VSC based multi-terminal DC system. Int J Electr Power Energy Syst 2021;132:107207. https://doi.org/10.1016/J.IJEPES.2021.107207.

[14] Yu JJQ, Hou Y, Lam AYS, Li VOK. Intelligent fault detection scheme for microgrids with wavelet-based deep neural networks. IEEE Trans Smart Grid 2019;10:1694–703. https://doi.org/10.1109/TSG.2017.2776310.

[15] Wu JY, Lan S, Xiao SJ, Bin YY. Single Pole-to-Ground Fault Location System for MMC-HVDC Transmission Lines Based on Active Pulse and CEEMDAN. IEEE Access 2021;9:42226–35. https://doi.org/10.1109/ACCESS.2021.3062703.

[16] Hadaeghi A, Samet H, Ghanbari T. Multi extreme learning machine approach for fault location in multi-terminal high-voltage direct current systems. Comput Electr Eng 2019;78:313–27. https://doi.org/10.1016/J.COMPELECENG.2019.07.022.

[17] Wu H, Wang Q, Yu K, Hu X, Ran M, Chen L. A novel intelligent fault identification method based on random forests for HVDC transmission lines. PLoS One 2020;15(3):e0230717.

[18] Ankar SJ, Yadav A. A novel approach to estimate fault location in current source converter–based HVDC transmission line by Gaussian process regression. Int J Electr Power Energy Syst 2020;30:12221. https://doi.org/10.1002/2050-7038.12221.

[19] Bhowmik PS, Purkait P, Bhattacharya K. A novel wavelet transform aided neural network based transmission line fault analysis method. Int J Electr Power Energy Syst 2009;31:213–9. https://doi.org/10.1016/J.IJEPES.2009.01.005.

[20] Deokar SA, Waghmare LM. Integrated DWT–FFT approach for detection and classification of power quality disturbances. Int J Electr Power Energy Syst 2014;61:594–605. https://doi.org/10.1016/J.IJEPES.2014.04.015.

[21] Rohani R, Koochaki A, Siahbalaee J. Fault Location in VSC-HVDC Systems Based on NSGA-II and Discrete Wavelet Transform. Int J Renew Energy Res 2022;12:1347–61. https://doi.org/10.20508/IJRER.V12I3.13050.G8519.

[22] Tonelli-Neto MS, Decanini JGMS, Lotufo ADP, Minussi CR. Fuzzy based methodologies comparison for high-impedance fault diagnosis in radial distribution feeders. IET Gener, Transm Distrib 2017;11:1557–65. https://doi.org/10.1049/IET-GTD.2016.1409.

[23] Mallat SG. A Theory for Multiresolution Signal Decomposition: The Wavelet Representation. IEEE Trans Pattern Anal Mach Intell 1989;11:674–93. https://doi.org/10.1109/34.192463.

[24] Übeyli ED. Combined neural network model employing wavelet coefficients for EEG signals classification. Digit Signal Process 2009;19:297–308. https://doi.org/10.1016/J.DSP.2008.07.004.

[25] Yazdani-Asrami M, Sadeghi A, Seyyedbarzegar S, Song W. DC Electro-Magneto-Mechanical Characterization of 2G HTS Tapes for Superconducting Cable in Magnet System Using Artificial Neural Networks. IEEE Tran Appl 2022;32(7):1–10.

[26] Jakšić O, Jakšić Z, Guha K, Silva AG, Laskar NM. Comparing artificial neural network algorithms for prediction of higher heating value for different types of biomass. Soft Comput 2023;27:5933–50. https://doi.org/10.1007/S00500-022-07641-4.

[27] Espinoza JL, Gonzalez LG, Sempertegui R. Micro grid laboratory as a tool for research on non-conventional energy sources in Ecuador. In: 2017 IEEE International Autumn Meeting on Power, Electronics and Computing, (ROPEC). p. 1–7.

[28] Kizilöz B. Prediction of daily failure rate using the serial triple diagram model and artificial neural network. Water Supply 2022; 22: 7040–58. https://doi.org/10.2166/WS.2022.315.

[29] Mellit A, Pavan AM. A 24-h forecast of solar irradiance using artificial neural network: Application for performance prediction of a grid-connected PV plant at Trieste. Italy Sol Energy 2010;84:807–21. https://doi.org/10.1016/J.SOLENER.2010.02.006.

[30] Li HZ, Guo S, Li CJ, Sun JQ. A hybrid annual power load forecasting model based on generalized regression neural network with fruit fly optimization algorithm. Knowl Based Syst 2013;37:378–87. https://doi.org/10.1016/J.KNOSYS.2012.08.015.

[31] Varanasi J, Tripathi MM. A hybrid model of generalized regression neural network and radial basis function neural network for wind power forecasting in Indian wind farms. J Manag Inf Syst 2020;23:49–63. https://doi.org/10.1080/09720510.2020.1721598.

[32] Xie Y, Li C, Lv Y, Yu C. Predicting lightning outages of transmission lines using generalized regression neural network. Appl Soft Comput J 2019;78:438–46. https://doi.org/10.1016/J.ASOC.2018.09.042.

[33] Reyes-Archundia E, Moreno-Goytia EL, Guardado JL. An algorithm based on traveling waves for transmission line protection in a TCSC environment. Int J Electr Power Energy Syst 2014;60:367–77. https://doi.org/10.1016/J.IJEPES.2014.03.022.

[34] Shafiullah M, AlShumayri KA, Alam MS. Machine learning tools for active distribution grid fault diagnosis. Adv Eng Soft 2022;173:103279. https://doi.org/10.1016/J.ADVENGSOFT.2022.103279.

[35] Geng M, Li Y, Ding B, Wang H. Deep Learning-based Cooperative Trail Following. In: 2018 International Joint Conference on Neural Networks (IJCNN 2018). p. 1–8.

[36] Rahmani A, Deihimi A. Reduction of harmonic monitors and estimation of voltage harmonics in distribution networks using wavelet analysis and NARX. Electr Power Syst Res 2020;178:106046. https://doi.org/10.1016/J.EPSR.2019.106046.

[37] Guo MF, Zeng XD, Chen DY, Yang NC. Deep-Learning-Based Earth Fault Detection Using Continuous Wavelet Transform and Convolutional Neural Network in Resonant Grounding Distribution Systems. IEEE Sens J 2018;18:1291–300. https://doi.org/10.1109/JSEN.2017.2776238.

[38] Shakiba FM, Azizi SM, Zhou M, Abusorrah A. Application of machine learning methods in fault detection and classification of power transmission lines: a survey. Artif Intell Rev 2022;56:5799–836. https://doi.org/10.1007/S10462-022-10296-0.

[39] Rao TCS, Ram SST, Subrahmanyam JBV. An effective technique for fault detection and classification in distribution system with the aid of DWT and ANFIS. Int J Autom Control 2017;11:411–27. https://doi.org/10.1504/IJAAC.2017.087055.

[40] Sadeh J, Afradi H. A new and accurate fault location algorithm for combined transmission lines using Adaptive Network-Based Fuzzy Inference System. Electr Power Syst Res 2009;79:1538–45. https://doi.org/10.1016/J.EPSR.2009.05.007.